Front. Struct. Civ. Eng. 2023, 17(2): 191–204
https://doi.org/10.1007/s11709-022-0906-1

RESEARCH ARTICLE

Safety assessment for buried drainage box culvert under influence of underground connected aisle blasting: A case study

Wenchang SUN[a], Nan JIANG[a*], Chuanbo ZHOU[a], Jinshan SUN[b], Tingyao WU[a]

[a] *Faculty of Engineering, China University of Geosciences, Wuhan 430074, China*
[b] *Hubei (Wuhan) Institute of Explosion and Blasting Technology, Jianghan University, Wuhan 430056, China*
[*] *Corresponding author. E-mail: jiangnan@cug.edu.cn*

ABSTRACT Blasting engineering in complex urban environments is considered to influence the safety and stability of the overlying drainage box culvert structure owing to vibration. Therefore, field blasting and vibration tests were performed on the blasting engineering of the Wuhan Metro Line 8 connected aisle, and the LS-DYNA software was used to analyze the dynamic response characteristics of an underground drainage box culvert during the blasting test. The vibration response evolution law of the buried drainage box culvert under blasting vibration was investigated, and a safe surface control standard for the blast vibration of a drainage box culvert is proposed. The results reveal that the maximum tensile stress of the box culvert structure was 0.33 MPa. The peak particle velocity (PPV) and peak tensile stress (PTS) of the drainage box culvert decreased as the water level in the box culvert increased. Based on the relationship between the tensile stress of the box culvert, PPV of the box culvert, and PPV of the surface, it is proposed that the surface control velocity of the buried drainage box culvert is 1.36 cm/s.

KEYWORDS drainage box culvert, underpass blasting, dynamic response, numerical simulation, safety assessment

1 Introduction

In recent years, with the development of urban rail transit construction in China, drilling and blasting methods have been widely used in the excavation of subway tunnels and their subsidiary structures. However, the dynamic response of an adjacent structure is often caused by explosives generated during blasting excavation. Damage and failure occur when the dynamic response exceeds the threshold value of the structure. As an indispensable part of the urban underground drainage system, the damage of the drainage box culvert has significant impact on the life and production of residents [1–4]. However, the safety control threshold of large-scale water supply and drainage box culvert structures has not been mentioned in the current Chinese safety blasting regulations.

To date, many studies in China and abroad have investigated the dynamic response characteristics of water drainage, supply culverts, and pipelines induced by blasting [5–7]. Yang et al. [8] investigated the dynamic response and damage development process of a reinforced concrete water conveyance box culvert under different working conditions based on a coupling model established by Lagrangian–Eulerian coupling. Based on field vibration tests and numerical simulations, Guan et al. [9] analyzed the horizontal and vertical dynamic response characteristics of horseshoe-shaped pipes under tunnel explosive loading. Based on blasting tests and numerical simulation methods, Yang et al. [10] analyzed the impact of the surface explosion load on a buried water diversion tank using a novel fully-coupled method. Jiang et al. [11] established a finite element numerical model to determine the dynamic response based on a model experiment, and investigated the response of the pipeline to impact loading under various mechanisms. He et al. [12] designed reciprocating loading tests with different variables for common pipeline materials in China, and investigated the failure characteristics and seismic

Article history: Received Jan 2, 2022; Accepted Aug 21, 2022

vulnerability of various pipeline types. The above-mentioned studies have investigated the dynamic response characteristics of culverts through field experiments.

With the development of numerical simulation software technology, studies have increasingly used numerical simulations to investigate the responses of drainage box culverts and pipelines. In terms of the water conveyance safety of large-scale box culverts, Cui et al. [13] simulated the interaction between water and box culverts based on numerical analysis technology, and analyzed the water conveyance safety of large-scale box culverts under blasting loads. Shahrin et al. [14] numerically investigated the blast-induced rock fragmentation response using the discrete element method (DEM) and particle blasting method (PBM). With regard to the dynamic response of a water supply pipeline, Xia et al. [15] evaluated the safety of a buried pipeline under explosive conditions during tunnel excavation based on a three-dimensional numerical engineering model and field testing. With regard to the dynamic response of buried gas pipelines, Jiang et al. [16] established a model of peak particle velocity (PPV) attenuation and combined it with a three-dimensional numerical model to establish a peak stress prediction model of pipeline explosives under different working conditions.

In summary, many studies have investigated buried water supply and drainage structures under blasting excavation. However, few studies have considered the blasting dynamic response for large-scale water supply and drainage box culvert structures. Actual engineering has shown that the dynamic response of the box culvert structure will differ according to different blasting excavation conditions and changes in the built-in water level of the drainage box culvert. Therefore, it is particularly important to investigate the dynamic response characteristics of the drainage box culvert under the influence of different blasting source distances and the built-in water level of the box culvert, and propose a corresponding safety control threshold. This paper presents a numerical modeling approach based on the blasting project of Xiaohongshan–Jiedaokou subway connected to the aisle of Wuhan Metro Line 8. Through a field blasting test and the numerical simulation of the drainage box culvert in this area, the dynamic response characteristics of the drainage box culvert were analyzed for different water levels and different excavation footages under blasting vibration. Combined with the stress control criteria of the drainage box culvert in the operating state, a safety control standard for the blasting vibration velocity of the drainage box culvert is proposed. The results obtained by this study have great significance as guidelines for engineering construction, and provide the foundation for establishing blasting safety control standards for similar structures.

2 Blasting engineering survey and field test

2.1 Project introduction

This project is located in the Xiaohongshan section of Wuhan Metro Line 8. The length of the station is 224.9 m, the total excavated area of the foundation pit is 5128.0 m^2, the depth of the foundation pit is 29.1–34.5 m, and the width of the standard section is 21.9 m. The excavation section of the connected aisle in the street section is a straight wall arch tunnel constructed using the mining method. The width is 3.8 m, the wall height is 3.3, the arch height is 1.9 m, the length is 34.25 m, and the excavation amount is 620 m^3. The drainage box culvert is located 3.4 m below the ground; the length is 30 m, the wall thickness is 0.4 m, and the culvert depth is 1.2 m. As shown in Fig. 1, the drainage box culvert is orthogonal to the connected aisle. This study mainly analyzed the influence of connected aisle excavation on the overlying drainage box culvert.

The stratum distribution is shown in Fig. 2. From the surface to the bottom, there are filled strata, clay strata, and limestone. The fill layer and clay stratum layer have a depth of 3.2 and 5.6 m, respectively.

In the blasting excavation process, the seismic effect caused by cutting-hole blasting is typically the strongest [17]. Here, wedge cutting was adopted according to the blasting design scheme, and the cutting holes were arranged in the upper steps. The tunnel blasting excavation cycle footage was 1 m, the cutting hole depth was 1.2 m, and the hole radius was 20 mm. The loading quantity of a single hole in the cut was 0.625 kg. The arrangement of the blast holes is shown in Fig. 3, and the parameters related to the blast hole are listed in Table 1.

2.2 Field blasting test and ground vibration monitoring analysis

A TC-4850 vibration monitor was used in the field tests.

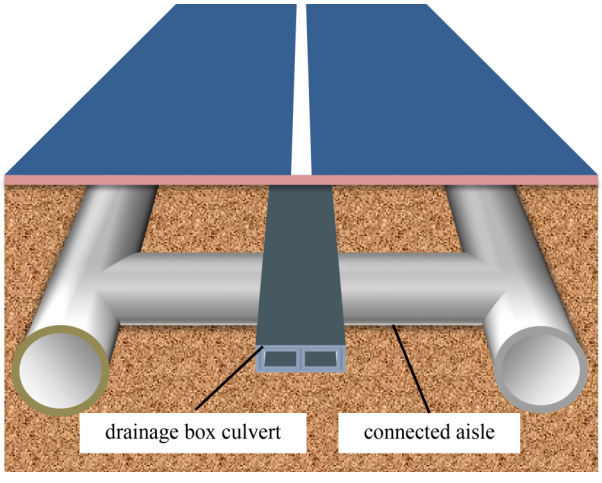

Fig. 1 Schematic diagram of relative position.

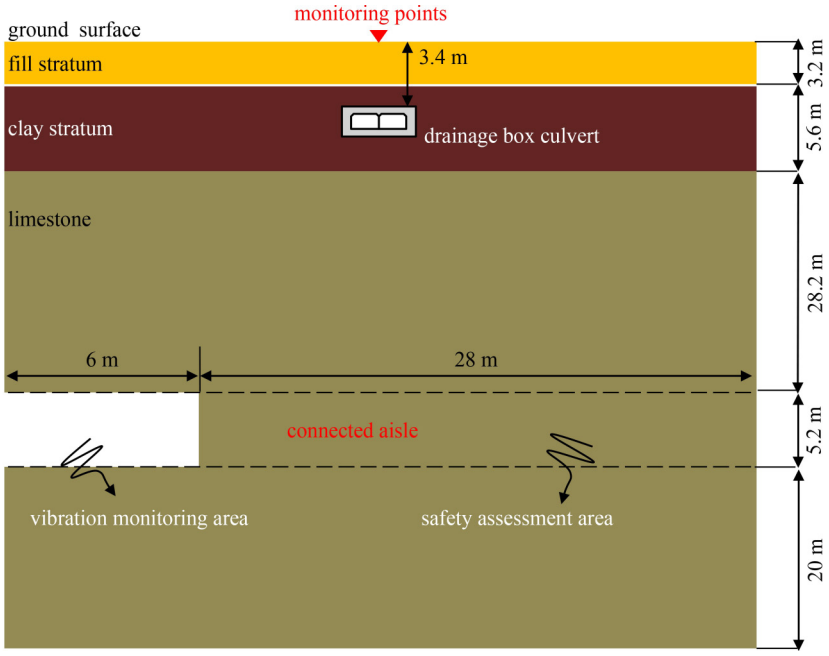

Fig. 2 Schematic diagram of stratum distribution.

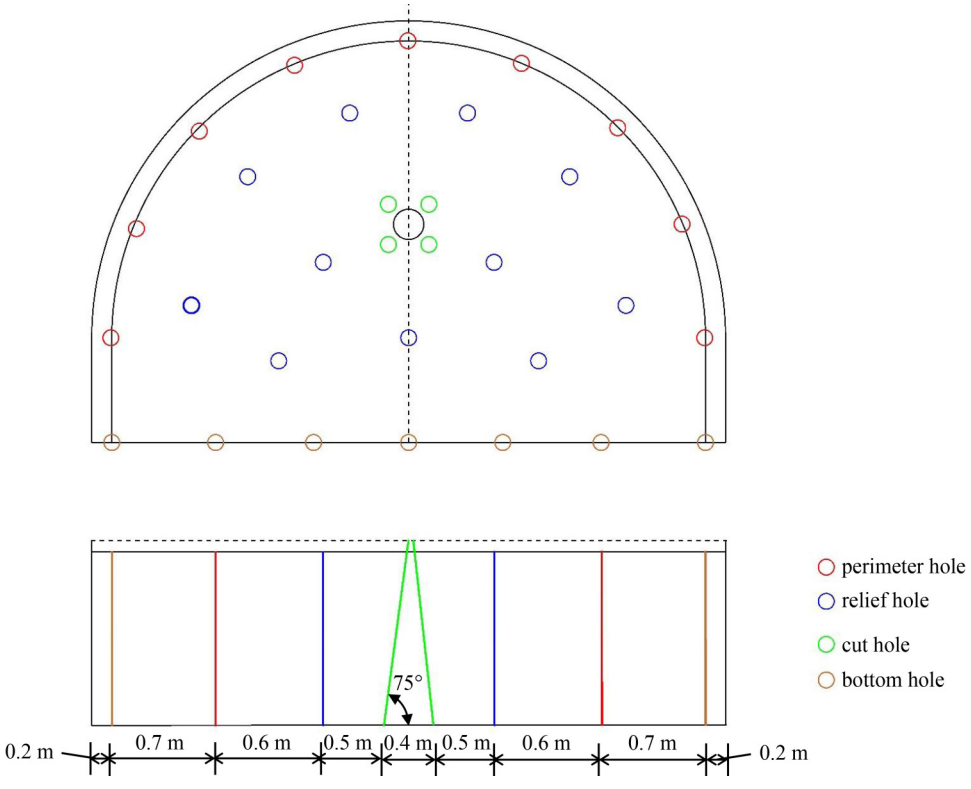

Fig. 3 Diagram of blast-hole arrangement.

To assess the influence of vibration on the drainage box culvert with satisfactory accuracy, the excavation footage section of 0–6 m was set as the blasting vibration test area, and the vibration monitoring of the blasting construction was carried out in this section. The excavation footage section of 6–34 m was set as the blasting safety assessment area. In practical engineering, the culvert of the drainage box is below the surface. However, because surface excavation is not practical for monitoring the vibration velocity of the drainage box culvert, the blasting vibration was monitored by arranging the instruments at different monitoring points on the surface above the drainage box culvert, as shown in Fig. 4. To ensure the accuracy of the results, five

Table 1 Blasthole parameters

blast holes category	type	depth (cm)	number of blast holes	charge of single hole (g)
relief hole	vertical	100	10	500
bottom hole	vertical	100	8	500
cut hole	15° inclined	120	4	625
perimeter hole	vertical	100	8	500
empty hole	vertical	100	1	0

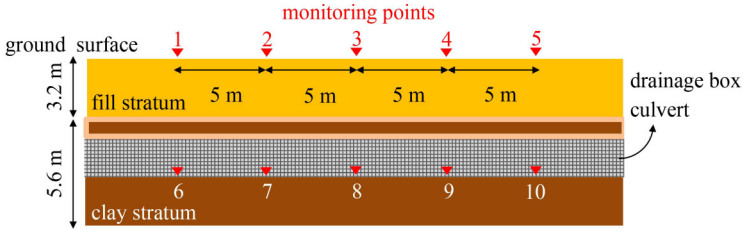

Fig. 4 Diagram of field monitoring point layout.

monitoring points were set to collect blasting vibration data. Figure 5 shows a photograph of the field monitoring setup.

To ensure the safety of the drainage box culvert under the blasting excavation of a connected aisle, a blasting experiment on the connected aisle was conducted before the blasting excavation. The blasting experiment was arranged according to the above-mentioned parameters of the blast-hole explosive. The PPV of the surface monitoring points was determined using the monitoring scheme described above. The blasting vibration data of monitoring points No. 2, No. 3, and No. 4 with an excavation footage of 2, 4, and 6 m were analyzed, and the results are presented in Table 2.

Based on the blasting test results, it is concluded that, as the excavation progressed, the resultant vibration velocity of the ground gradually increased. In the three blasting tests, the maximum resultant vibration velocity was 0.201 cm/s under the 6-m working condition. In practical engineering applications, the following models are used to predict the particle vibration velocity when a

Fig. 5 Diagram of field monitoring setup.

vibration wave propagates to soil [18]:

$$v = 51.412\left(\frac{\sqrt[3]{Q}}{r}\right)^{1.126}\left(\frac{d}{r}\right)^{0.722}, \quad (1)$$

where v is the vibration velocity, Q is the maximum dose of a single segment, r is the phase-burst distance, and d is the tube diameter.

Table 2 Results of blasting experiment

excavation footage	monitoring point number	X-axis (cm·s^{-1})	Y-axis (cm·s^{-1})	Z-axis (cm·s^{-1})	resultant vibration velocity (cm·s^{-1})
2 m	2	0.034	0.122	0.072	0.124
	3	0.044	0.135	0.062	0.131
	4	0.036	0.119	0.068	0.121
4 m	2	0.073	0.131	0.069	0.135
	3	0.054	0.148	0.073	0.143
	4	0.063	0.126	0.089	0.129
6 m	2	0.082	0.154	0.123	0.161
	3	0.091	0.198	0.135	0.201
	4	0.085	0.170	0.141	0.165

3 Dynamic numerical calculation model and verification

3.1 Model size and boundary conditions

To investigate the dynamic response of the drainage box culvert under blasting, the LS-DYNA numerical simulation software was used. The model adopts a solid element. The drainage box culvert was buried in a clay layer with a thickness of 3.2 m. The buried depth of the drainage box culvert was 3.4 m. The overall size of the model is 30 m × 62.2 m × 34.25 m. The explosive, surrounding rock, stemming, soil, and drainage box culverts were divided using a Lagrangian grid. Considering the fluid–solid coupling between the water and drainage box culvert, non-co-nodes were set on the contact surface of the water and drainage box culvert. The fluid–solid coupling algorithm was added to the *K* file [19,20]. The surface ground of the model adopted a free boundary, and all other interfaces were non-reflective boundaries. The numerical model and drainage box culvert mesh diagram are shown in Fig. 6.

3.2 Calculation of constitutive model and parameter

The No. 2 rock emulsion explosive was used for the site. The relationship between the pressure and specific volume is described by the Jones−Wilkens−Lee (JWL) state equation [21–23], as follows:

$$P = A\left(1-\frac{\omega}{R_1 V}\right)\mathrm{e}^{-R_1 V} + B\left(1-\frac{\omega}{R_2 V}\right)\mathrm{e}^{-R_2 V} + \frac{\omega E_0}{V}, \quad (2)$$

where A, B, R_1, R_2, and ω are material constants; P is the pressure; V is the relative volume; and E_0 is the initial specific internal energy. The blasting material parameters are listed in Table 3.

According to the site construction characteristics, the *MAT_DRUCKER_PRAGER model was adopted in the fill and clay strata of the model [24–26]. The yield surface constructed by the Drucker–Prager yield criterion model can accurately simulate the mechanical properties of the soil [27]. The plastic potential function is expressed as follows:

$$f = \alpha I_1(\sigma_{ij}) + \sqrt{I_2(\sigma_{ij})} + k = 0, \quad (3)$$

where f is a potential function; $I_1(\sigma_{ij})$ is the first stress tensor invariance; $I_2(\sigma_{ij})$ is the second stress tensor invariance; α and k are constants.

The *MAT_PLASTIC_KINEMATIC model was adopted for slightly weathered mudstone and stemming [28]. The relationship between the stress and strain of this model is expressed as follows:

$$\sigma_y = \left(1+\frac{\varepsilon^{\frac{1}{P}}}{C}\right)\left(\sigma_0 + \beta E_P \varepsilon_P^{\mathrm{eff}}\right), \quad (4)$$

where σ_y is the initial yield stress; ε is the strain rate; C and P are variable quantities; $\varepsilon_P^{\mathrm{eff}}$ is the effective plastic strain; E_p is the plastic hardening modulus; β is the hardening factor.

The calculation parameters of the related models are listed in Table 4.

Water was introduced using the keyword *MAT_NULL. The state equation is defined by *EOS_GRUNEISEN [29–31], as follows:

$$\begin{cases} P = \dfrac{\rho_0 C^2 \mu\left[1+\left(1-\dfrac{\gamma_0}{2}\right)\mu - \dfrac{a}{2}\mu^2\right]}{\left[1-(S_1-1)\mu - S_2\dfrac{\mu^2}{\mu+1} - S_3\dfrac{\mu^3}{(\mu+1)^2}\right]} + (\gamma_0 + a\mu)E, & \mu > 0 \\ P = \rho_0 C^2 \mu + (\gamma_0 + a\mu)E, & \mu < 0 \end{cases} \quad (5)$$

where C is the sound speed underwater; $\mu = \rho/\rho_0 - 1$; ρ is the water disturbance density; ρ_0 is the initial density; E is the energy; γ_0 is the GRUNEISEN coefficient; S_1, S_2, and S_3 are slope coefficients; α is the volume correction coefficient. The specific parameters are listed in Table 5.

Because it is difficult to establish a reinforced concrete

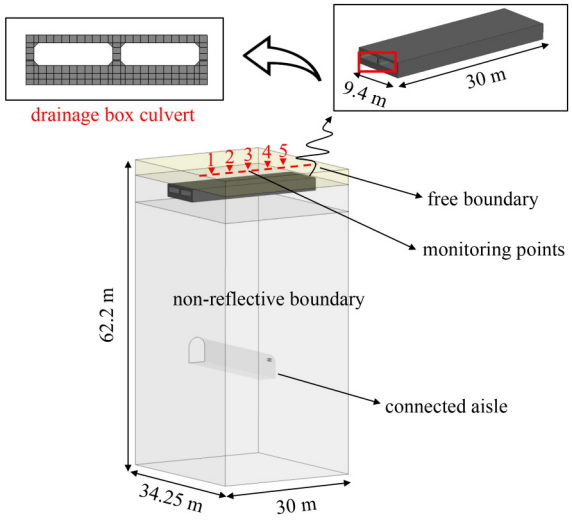

Fig. 6 Diagram of numerical model and drainage box culvert.

Table 3 Parameters of blasting material

density (g·cm^{-3})	bursting velocity (m·s^{-1})	bursting pressure (GPa)	A (GPa)	B (GPa)	R_1	R_2	E_0 (GPa)
1.15	3300	3.24	214	18.2	4.2	0.9	4.19

Table 4 Material parameters used in calculation

type	P (g·cm^{-3})	elastic modulus (GPa)	shear modulus (GPa)	Poisson's ratio	cohesion (MPa)	internal friction angle (°)	tensile strength (MPa)
fill stratum	1.98	0.027	0.009	0.34	0.1	10	0.016
silty clay	1.95	0.039	0.015	0.25	0.25	15	0.028
stemming	0.85	0.18×10^{-3}	–	0.35	–	–	–
slightly weathered mudstone	2.68	7	3.09	0.25	5.5	43	2.58

Table 5 Parameters of water material model

density (g·cm^{-3})	sound velocity (m·s^{-1})	S_1	S_2	S_3	γ_0
1.0	1500	2.55	1.976	1.227	0.49

model of the drainage box culvert using a finite element approach, the equivalent modulus was used to model the material of the drainage box culvert [32]. The drainage box culvert was modeled using *MAT_JOHNSON_HOLMQUIST_CONCRETE. The constitutive equation is expressed as follows:

$$\sigma^* = \left[A(1-D)+Bp^{*n}\right](1+c\ln\varepsilon^*), \tag{6}$$

where A, B, and n are constants; $\sigma^* = \sigma/f$ is the ratio of the actual equivalent stress to the static yield strength; D ($0 \leqslant D \leqslant 1$) is the damage factor; $p^* = p/f'$ is the dimensionless pressure; $\varepsilon^* = \varepsilon/\varepsilon_0$ is the dimensionless strain rate.

4 Dynamic response and safety evaluation of blasting test

4.1 Reliability analysis of ground vibration distribution and calculation model during test

All elements along the culvert body and surface were selected in the numerical model to investigate the spatial distribution characteristics of the vibration velocity on the drainage box culvert during the blasting process. The PPV distribution of the resultant velocity is shown in Fig. 7. As can be seen, under the three blasting test conditions, the PPV of the box culvert (v_d) and the PPV of the surface (v_g) exhibited a decreasing trend from the central section to both ends of the box culvert. The box culvert center is the most dangerous area. The vibration velocity was maximum when the excavation footage was 6 m, which is consistent with the actual project situation. Then, the monitoring points corresponding to Fig. 5 were selected to compare the vibration velocity in the numerical simulation to that in the field test.

Table 6 presents the PPV comparison in the X-, Y-, and Z-directions of the monitoring and numerical simulation. As can be seen, the maximum error of the resultant vibration velocity is 10.44%, and the minimum error is 5.85%. The numerical simulation revealed that the maximum vibration velocity is 0.201 cm/s, while that of field monitoring is 0.182 cm/s. These two peaks appeared at monitoring point No. 3. The results are consistent, indicating the accuracy of the numerical model. Therefore, it is feasible to investigate the response of a drainage box culvert under blasting using numerical simulation. Moreover, the simulation results reveal that the vibration velocity decreases as the distance from the explosion source increases. The maximum vibration velocity point appeared immediately above the explosion source.

To further verify the accuracy of the numerical data, the vibration velocity of monitoring point No. 3 was analyzed. The vibration velocity-time history curve obtained by field monitoring and numerical simulation is shown in Fig. 8. As can be seen, the measured velocity–time curve is in good agreement with the time

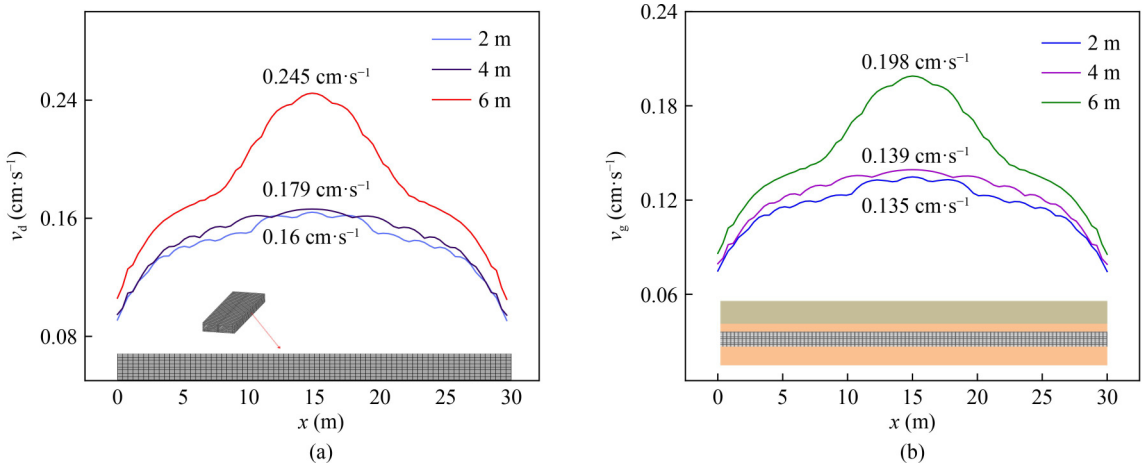

Fig. 7 Distribution characteristics of PPV. (a) Ground-monitoring points; (b) drainage-box culvert monitoring points.

Table 6 Vibration velocity in field test and numerical simulation

monitoring point	numerical simulation ($cm \cdot s^{-1}$)				field test ($cm \cdot s^{-1}$)				resultant PPV error
	X-PPV	*Y*-PPV	*Z*-PPV	resultant PPV	*X*-PPV	*Y*-PPV	*Z*-PPV	resultant PPV	
#1	0.054	0.129	0.119	0.136	0.042	0.118	0.110	0.122	9.93%
#2	0.082	0.154	0.123	0.161	0.078	0.150	0.158	0.171	5.85%
#3	0.091	0.198	0.135	0.201	0.089	0.179	0.171	0.182	10.44%
#4	0.085	0.158	0.141	0.165	0.063	0.175	0.159	0.177	6.78%
#5	0.051	0.133	0.121	0.135	0.056	0.119	0.118	0.124	7.26%

history curve of the numerical simulation, which confirms the reliability of the numerical model. Additionally, the vibration propagation laws of the blasting seismic wave revealed by the two methods are essentially identical. The vibration velocity of the numerical simulation first reached the PPV, but the time delay of the peak monitoring velocity was only 0.02 s. The PPV of the numerical simulation is larger than that obtained by the field tests, because the geological conditions at the site are more complex. The numerical simulation simplified the formation material to a certain extent. In practice, the complex geological conditions in the formation weaken the blasting seismic wave to a certain extent, resulting in smaller PPV. Hence, the vibration frequencies of the numerical simulation and field test are slightly different.

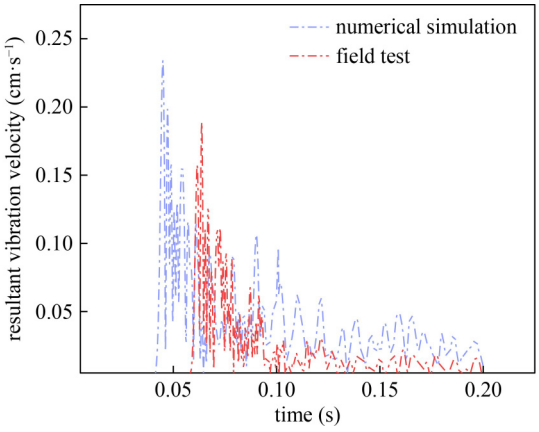

Fig. 8 Comparison diagram of resultant vibration velocity.

4.2 Dynamic response characteristics of box culvert during test

Figure 9 shows the propagation characteristics of seismic waves in the stratum media. As shown in Fig. 9(a), the seismic wave propagated around the spherical waves after blasting. As shown in Fig. 9(b), as the spread proceeded, the scope of the wave increased, and the peak pressure decreased. Additionally, it can be observed that reflection does not occur when the seismic wave is transmitted to the boundary, which explains the correctness of the boundary condition setting. The seismic wave reached the junction of the rock medium and soil layer at 43999 μs. Figure 9(d) shows that some waves propagated to the bottom at the interface between the rock mass medium and soil layer, while others propagated upward through the interface. Blasting seismic waves have complex reflections and transmissions when propagating in different media such as rock, soil, box culverts, and water. With time, the wave decays, and the peak stress decreases. When the seismic wave in the soil layer decays completely, the dynamic response of the drainage box culvert stops.

Owing to the inconvenience of excavating an underground drainage box culvert, the vibration velocity of a drainage box culvert cannot be tested in practical engineering. In blasting vibration monitoring, the ground vibration velocity near the drainage box culvert is used to reflect the vibration velocity of the drainage box culvert. In this study, the PPV of the drainage box culvert and surface was fitted according to the monitoring data and numerical model. The drainage box culvert and ground PPV statistics with an excavation footage of 6 m are shown in Fig. 10. As can be seen, there is a functional relationship between the drainage box culvert and the ground vibration velocity, and the relationship between them can be expressed as follows:

$$v_d = 1.075 v_g, \tag{7}$$

where v_d is the PPV of the drainage box culvert, and v_g is the surface PPV ($cm \cdot s^{-1}$).

$$R = \frac{v_d}{v_g}. \tag{8}$$

4.3 Safety evaluation of drainage box culvert during test

Figure 11 shows the stress–time curves of the back blast surface and blast surface at an excavation footage of 6 m. A compressive stress zone first appeared on the blast surface. Subsequently, the tensile stress area lagged behind at the back, indicating that the seismic wave first reached the bottom plate of the box culvert. As the blasting advanced, the stress zones alternately changed, indicating that the waves propagated along the vertical and horizontal directions of the drainage box culvert. The stress on the drainage box culvert increased continuously, and the back blast surface and blast surface reached the

peak tensile stress and compressive stress, respectively. Subsequently, the maximum stress of the seismic wave continuously decreased. When the seismic wave had completely attenuated in the drainage box culvert, the dynamic response of the drainage box culvert stopped.

To intuitively reflect the dynamic response characteristics of the drainage box culvert, Fig. 12 shows the stress change process of the blast surface of the drainage box culvert with an excavation footage of 6 m. As can be seen, after 43999 μs, the blasting seismic wave started acting on the drainage box culvert. The action position was on the blast surface of the box culvert, opposite to the blast source. A compressive stress zone first appeared on the blast side. With seismic wave action, a compressive stress zone developed along the length direction of the drainage box culvert on both sides, and tensile and compressive stress zones appeared alternately.

Figure 13 shows the stress change process of the back-

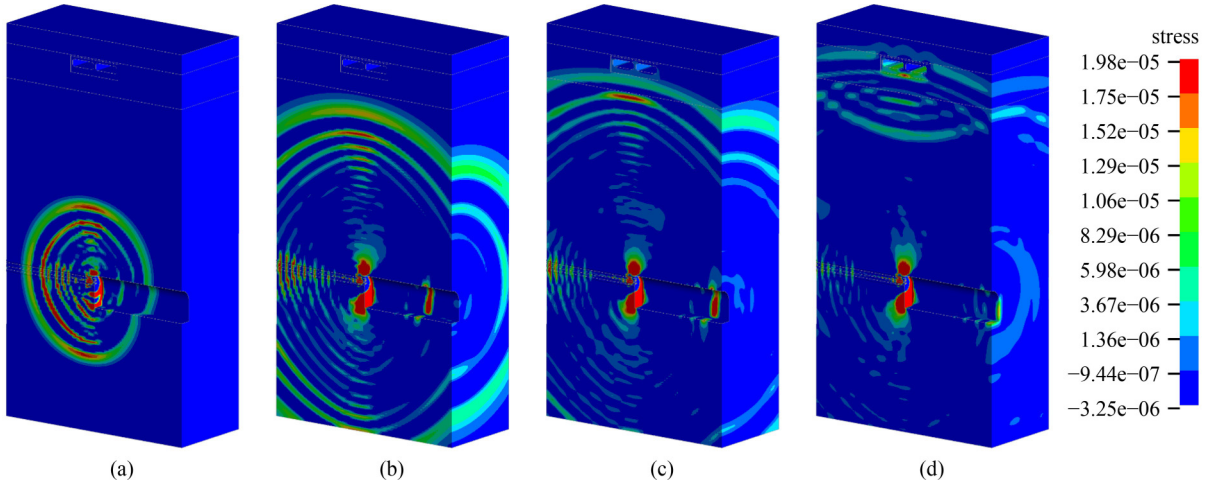

Fig. 9 Propagation of blasting seismic wave. (a) 23999 μs; (b) 33999 μs; (c) 43999 μs; (d) 53999 μs.

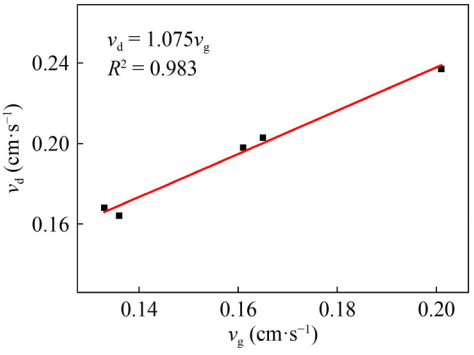

Fig. 10 Schematic diagram of relationship between drainage box culvert and surface vibration velocity.

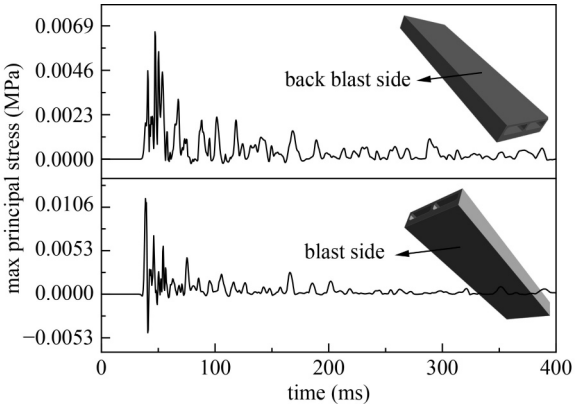

Fig. 11 Back blast surface and blast surface stress curve.

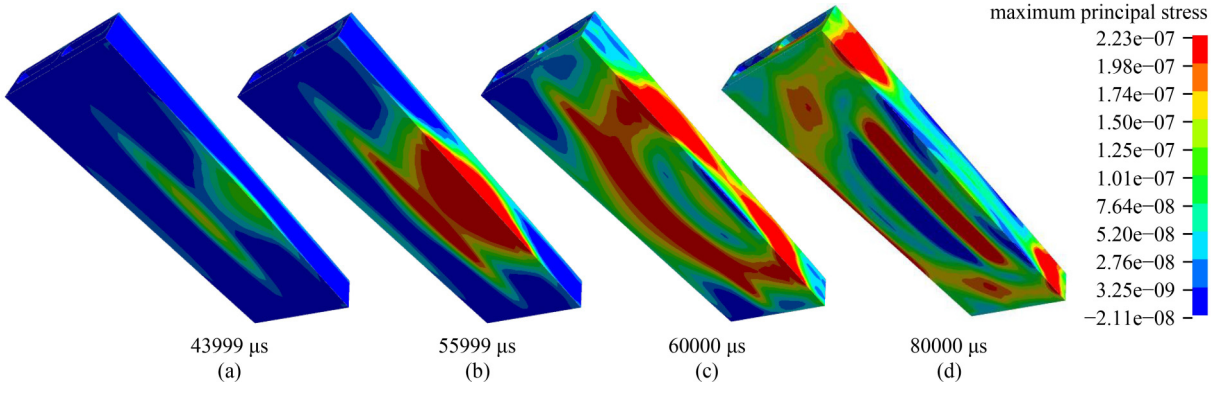

Fig. 12 Tensile stress evolution of blast surface. (a) 43999 μs; (b) 55999 μs; (c) 60000 μs; (d) 80000 μs.

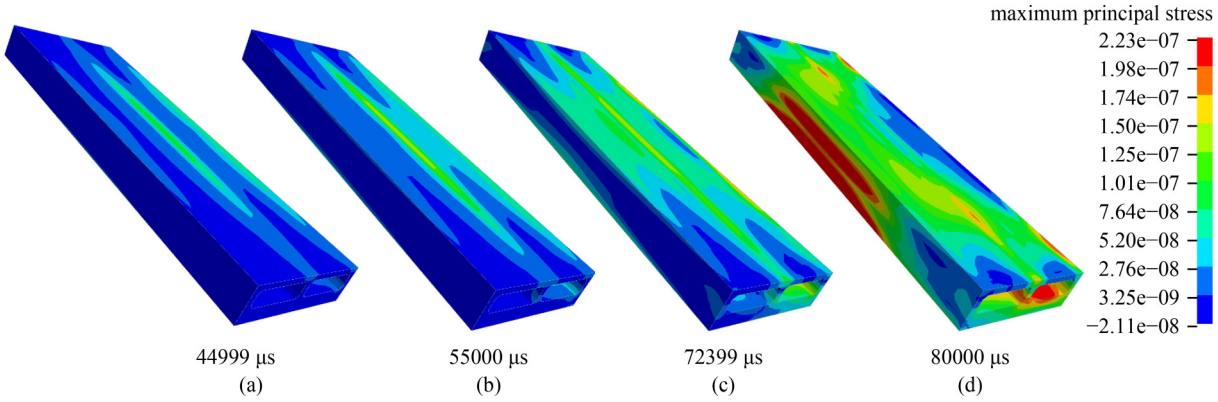

Fig. 13 Tensile stress evolution of back blast surface. (a) 44999 μs; (b) 55000 μs; (c) 72399 μs; (d) 80000 μs.

blast surface of the drainage box culvert when the excavation footage was 6 m. As can be seen, the stress zone of the back-blast surface appeared later than that of the blast surface. As the blasting seismic wave spread, the tensile stress peak zone first appeared at the part of the back blast surface facing explosive at 55000 μs. The stress was significantly larger than that of the other stress zones. Subsequently, the stress zone developed up to the length of the drainage box culvert.

Figure 14 shows the peak tensile stress (PTS) contour of the drainage box culvert section immediately above the explosion source when the excavation footage was 6 m. As can be seen, the PTS at the four chamfers is maximum at 0.29, 0.24, 0.26, and 0.33 MPa, respectively. The PTS at other positions is obviously smaller than the tensile stresses at the chamfers on both sides. The tensile stress on the blast side of the drainage box culvert is generally higher than that on the back. The PTS at the bottom of the drainage box culvert is 0.23 MPa, while the PTS at the top is 0.06 MPa. Considering the particularity of the chamfer structure of the drainage box culvert, there is a certain degree of stress concentration. Therefore, the stress is larger at the chamfer position. According to the GB50010-2010 specification, the tensile strength standard for C30 concrete is 2.00 MPa [33]. Under this condition, the maximum tensile stress of the drainage box culvert is far less than the tensile strength professional criterion. Moreover, box culvert leakage was not observed during the field blasting process, which indicates that the drainage box culvert is safe when the excavation footage is 6 m.

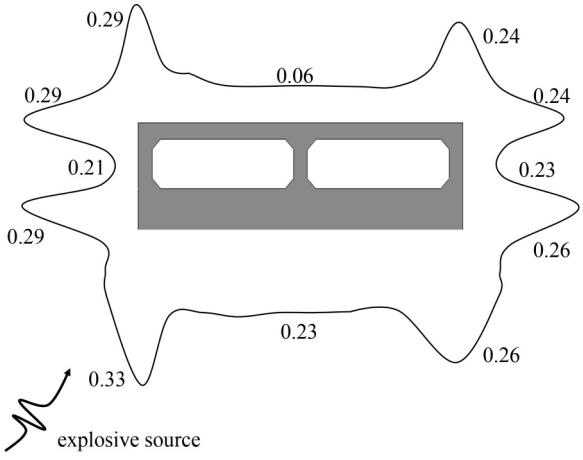

Fig. 14 Stress distribution in different parts of box culvert.

5 Structural safety prediction of underpass blasting process

With the excavation of the tunnel facing forward, the distance between the blasting area and the drainage box culvert gradually decreased. In practical engineering, the drainage box culvert operates under underwater conditions. Therefore, the parameters verified above and numerical calculation methods were used to establish three-dimensional calculation models under different conditions, and these models were then used to investigate the influence of blasting on the drainage box culvert during a water-filling operation. The schematic diagrams of the numerical models for the five different excavation footages are shown in Fig. 15.

5.1 Evolution law of structural vibration response under different footage

5.1.1 Evolution law of vibration velocity under different excavation footage

Figure 16 shows the evolution of PPV in different parts of the drainage box culvert under five types of excavation footage: 7, 12, 17, 22, and 27 m. As can be seen, the maximum PPV in the most dangerous section of the drainage box culvert changed with the excavation footage. The same law applies for all working conditions before 17 m. The maximum vibration velocity occurred at point G and the minimum vibration velocity occurred at point C. After 17 m, all working conditions obeyed the same law. The maximum vibration velocity occurred at

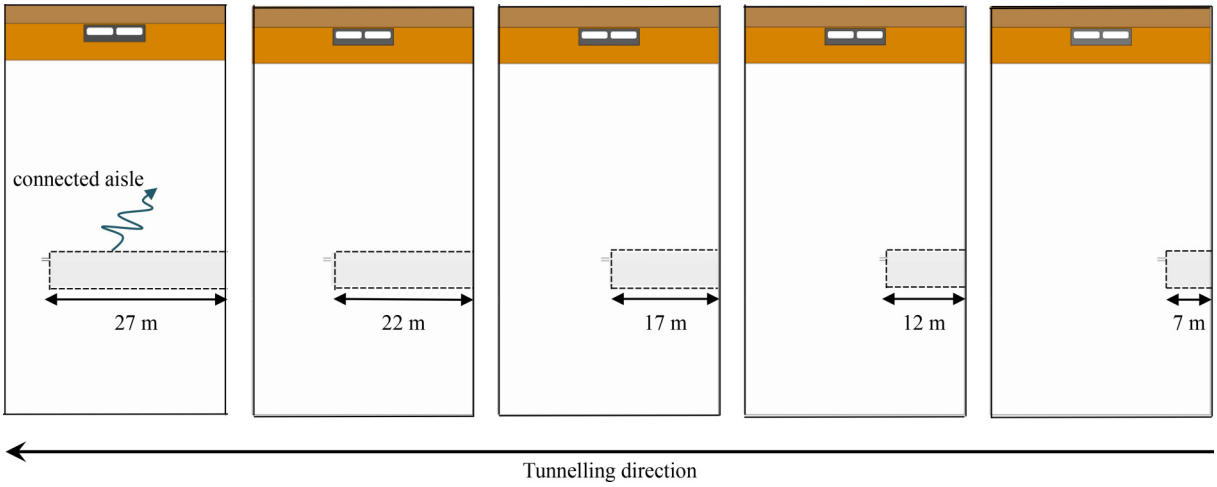

Fig. 15 Numerical models of different excavation footages.

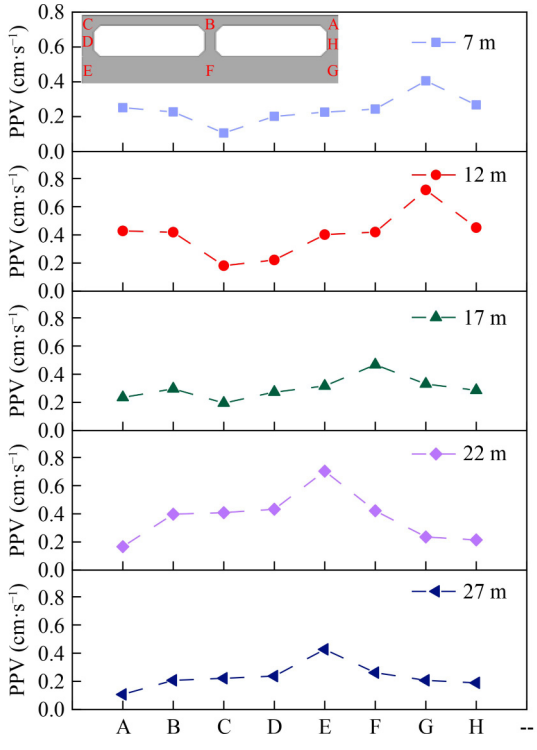

Fig. 16 Influence of different excavation footage on PPV of drainage box culvert.

point E, and the minimum PPV occurred at point A. As the excavation progressed, the variation range of each part of the box culvert was different. Overall, the variation range of the PPV of the side wall and top of the box culvert is small: the maximum variation range of the side wall is 0.2 cm/s, the maximum variation range of the top is 0.25 cm/s, and the maximum variation range of the bottom is 0.43 cm/s. As can be seen, the change in excavation footage had the greatest influence on the bottom of the box culvert, whereas the influence on the top and side walls was small and without an obvious cavity effect.

5.1.2 Evolution law of tensile stress under different excavation footage

The five working conditions of 7, 12, 17, 22, and 27 m were considered to investigate the evolution law of the box culvert tensile stress. The evolution law of the PTS of the drainage box culvert for the different excavation footage types is shown in Fig. 17. As can be seen, the PTS of the box culvert varied significantly. As the excavation footage increased, the PTS of the box culvert first increased and then decreased. When the excavation footage was 12 m, the PTS reached its maximum value. A

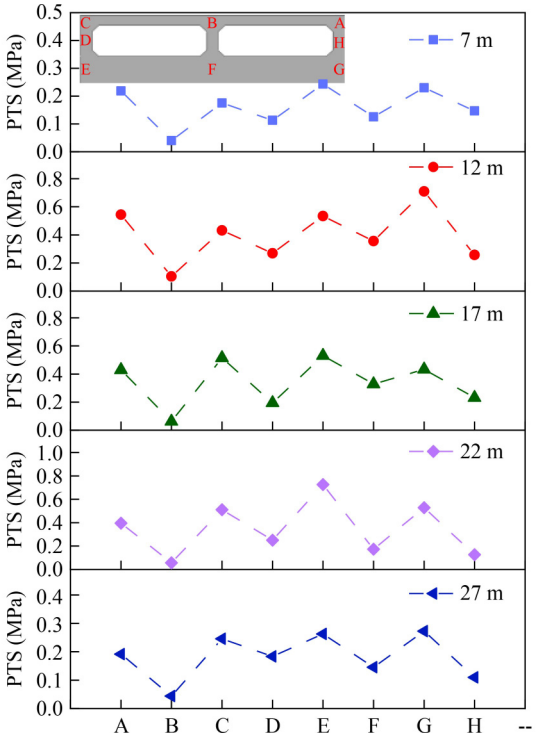

Fig. 17 Influence of different excavation footage on PTS of drainage box culvert.

change in the excavation footage will change the location of the maximum tensile stress. As the excavation footage changed, the PTS appeared at the chamfer closest to the explosion source. The PTS at the chamfer was larger than that at the surrounding position. The PTS of A, C, E, and G was larger than that of other parts under different excavation footages. The PTS of A and E was larger at 7 and 12 m, and the difference was small. When the working conditions were 17, 22, and 27 m, both C and E exhibited large PTS. When the working condition was 17 m, the PTS at C was significantly greater than that at E. When the working conditions were 22 and 27 m, the difference was insignificant. As the excavation footage changed, the PTS varied at different locations. Overall, the changes at the middle and top of the culvert were significantly smaller than those at the bottom.

5.2 Evolution law of dynamic response under different operating conditions

In practice, the drainage box culvert operates under water-filling conditions. Therefore, to better suit the working conditions, models of the $H/4$, $H/2$, $3H/4$, and full water levels under different excavation footages were established in LS-DYNA. The model diagram is shown in Fig. 18. To analyze the evolution law, 25 different working conditions were established with the model under the above-mentioned empty water state.

5.2.1 Vibration velocity evolution of drainage box culvert

As discussed in Subsection 3.1, the middle part of the drainage box culvert is the most dangerous. The resultant vibration velocity of this part under the 25 conditions is plotted in Fig. 19. As can be seen, the PPV of the drainage box culvert was maximum under the empty water condition. As the water level increased, the PPV of the most dangerous section decreased, and the minimum value was 0.281 cm/s under the full water condition. The water level influence on the PPV is different for different footages. The PPV differences between the empty water and full water conditions at the five excavation footages of 7, 12, 17, 22, and 27 m are 0.072, 0.138, 0.087, 0.062, and 0.056 cm/s, respectively.

5.2.2 Tensile stress evolution of drainage box culvert

The most dangerous part of the drainage box culvert was selected. The position of the maximum PTS at each excavation footage was selected from the above results to analyze the PTS at different water levels. As shown in Fig. 20, as the water level increased, the PTS decreased continuously. Therefore, a drainage box culvert is safer when operating under full water conditions. In the case of the water-filling operation, water has an effect similar to damping, that is, it diminishes the effect of the blasting

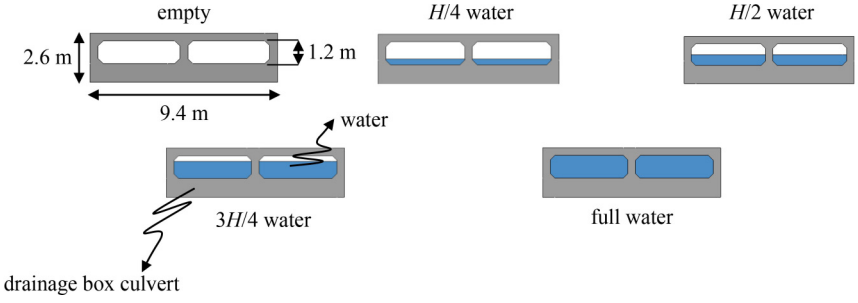

Fig. 18 Schematic diagram of different water level models.

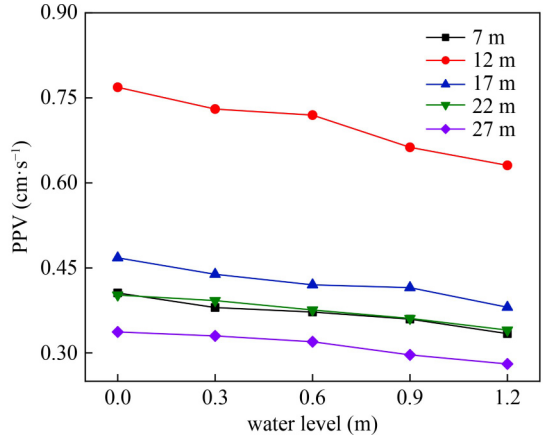

Fig. 19 Evolution of PPV under different working conditions.

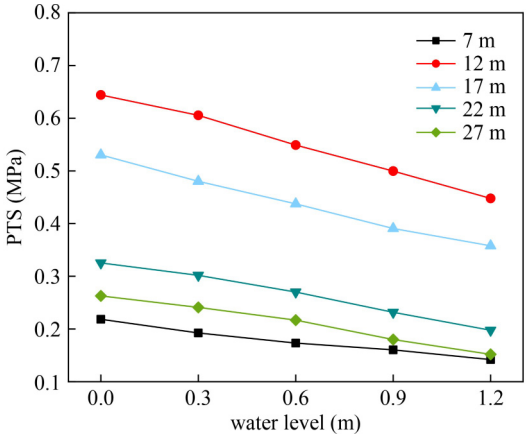

Fig. 20 Evolution of PTS under different working conditions.

shock wave on the drainage box culvert. Additionally, different water levels have different influence on the PTS under different excavation footages. The PTS changes for the empty water and full water states under the five working conditions of 7, 12, 17, 22, and 27 m are 0.076, 0.196, 0.172, 0.128, and 0.111 MPa, respectively. Water was found to have significant influence on the PTS when the explosion source was under the drainage box culvert.

6 Safety evaluation standard of drainage box culvert

Damage to underground buildings or structures under blasting seismic waves is often caused by stresses exceeding the material strength. Currently, there are many methods for controlling the influence of blasting vibration on buildings or structures, mainly by controlling the vibration velocity. According to the analysis results discussed above, the PTS of the box culvert on A and E is larger, therefore, these two locations are vulnerable. The PPV at A is larger than that at E, therefore, the PPV at A was used as the PPV safety criterion for the entire box culvert. According to Figs. 14 and 15, the PPV and PTS at A were analyzed under the empty water condition and with different excavation footages. The mathematical relationship between the PPV and PTS, shown in Fig. 21, is obtained as follows:

$$\sigma_T = 1.848 v_d - 0.246, \tag{9}$$

where σ_T is the PTS (MPa) and v_d is the PPV of the box culvert (cm/s).

According to Fig. 21, $R^2 = 0.947$, which indicates that the PPV of the drainage box culvert has a linear relationship with the PTS. By substituting Eq. (9) into Eq. (8), the following relationship between the drainage box culvert tensile stress and ground surface vibration velocity can be obtained:

$$v_g = \frac{\sigma_T + 0.246}{1.848R}. \tag{10}$$

According to the tensile strength of the concrete material of the box culvert, the safety control vibration velocity of the surface under explosive conditions can be obtained using the maximum tensile stress intensity theory. By introducing the standard tensile strength of 2.00 MPa for C30 concrete into Eq. (10), the safety threshold statistics of the box culvert and peak ground vibration velocity under different water levels were obtained as presented in Table 7.

From Table 7, it can be found that, the safety threshold of PPV increases with the water level in the drainage box culvert, which further indicates that the box culvert underwater filling operation is safer. In summary, the PPV of the surface soil is often used as monitoring data,

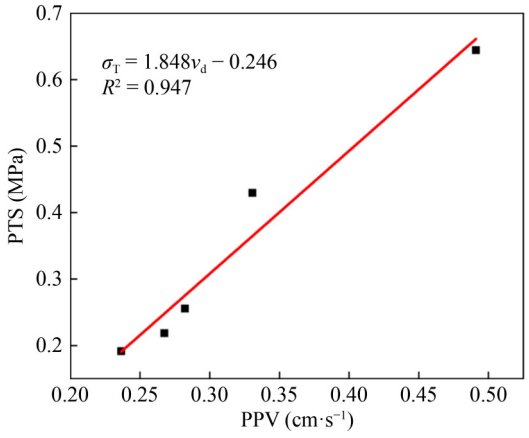

Fig. 21 Schematic diagram of relationship between PPV and PTS.

Table 7 Safety threshold of vibration velocity at different water levels

water level (m)	safety threshold of box culvert PPV (cm·s^{-1})	safety threshold of surface PPV (cm·s^{-1})
0	1.21	0.71
0.3	1.38	0.81
0.6	1.62	0.95
0.9	1.91	1.12
1.2	2.32	1.36

because the box culvert is not easy to excavate in practice. In practical blasting engineering, the drainage box culvert underwater filling operation is safer. The surface safety control velocity at the full water state is 1.36 cm/s, which is a reasonable safety control velocity for the drainage box culvert during operation.

7 Conclusions

Based on vibration monitoring and numerical engineering simulation, this study investigated the impact of connected aisle vibration blasting on a drainage box culvert. The main conclusions are as follows.

1) Under the influence of explosives, the PPV of the surface above the explosive source was maximum. With the explosion source as the center, as the distance along the length direction of the box culvert increased, the PPV of the ground decreased.

2) The numerical simulation revealed that, along the box culvert direction, the PPV first increased and then decreased. The PPV was maximum at the middle of the box culvert, that is, the position above the explosive. Therefore, the middle of the drainage box culvert is the most dangerous. In the most dangerous section of the drainage box culvert, the maximum PTS appeared at the chamfer of the culvert, whereas the maximum PPV appeared at the bottom of the culvert.

3) Through numerical simulation analysis, the PTS and PPV at the most dangerous section of the drainage box culvert were small when the connected aisle passed through the drainage box culvert. Therefore, it is considered that the influence of the explosives on the drainage culvert is limited and that the drainage box culvert is safe.

4) The water in the box culvert plays a damping role and weakens the effect of blasting shock waves. As the water level rose in the drainage box culvert, the PPV and PTS of each part of the culvert gradually decreased. According to the maximum tensile stress intensity theory, the surface safety control speed of the box culvert under operation was 1.36 cm/s.

Acknowledgements The study was sponsored by the National Natural Science Foundation of China (Grant Nos. 41807265, 41972286, and 42072309), and the Hubei Key Laboratory of Blasting Engineering Foundation (Nos. HKLBEF202001 and HKLBEF202002).

References

1. Zhang Y Q, Jiang N, Zhou C B, Wu T Y, Luo X D, Xia Y Q. Study on dynamic response of building structures adjacent to high-rise frames caused by blasting vibration of subway foundation pit. Journal of Sustainable Mining, 2017, 16(4): 179−188
2. Wang K X, Hu P, Zhou J X. Study on fatigue damage and safety location of adjacent building structure under frequent mine earthquake. Journal of Safety Science and Technology, 2021, 17(06): 58−64
3. Sołtys A, Twardosz M, Winzer J. Control and documentation studies of the impact of blasting on buildings in the surroundings of open pit mines. Journal of the China Coal Society, 2019, 44(S1): 118−125
4. Zhu H, Wang X, Wang Y, Ji C, Wu G, Zhang L, Han Z. Damage behavior and assessment of polyurea sprayed reinforced clay brick masonry walls subjected to close-in blast loads. International Journal of Impact Engineering, 2022, 167: 104283
5. Kheradi H, Nagano K, Nishi H, Zhang F. 1-g shaking table tests on seismic enhancement of existing box culvert with partial ground-improvement method and its 2D dynamic simulation. Soil and Foundation, 2018, 58(3): 563−581
6. Yatsumoto H, Mitsuyoshi Y, Sawamura Y, Kimura M. Evaluation of seismic behavior of box culvert buried in the ground through centrifuge model tests and numerical analysis. Underground Space, 2019, 4(2): 147−167
7. Lu X, Liu Y, Zhang L L. Research on deformation characteristics of tunnel box culvert structure under different construction loads. IOP Conference Series. Earth and Environmental Science, 2021, 634(1): 012136
8. Yang G D, Wang G H, Lu W B, Zhao X H, Yan P. Damage assessment and protection effect analysis of large water conveyance box culvert under the action of surface explosion load. Journal of Vibration and Shock, 2019, 38(5): 28−37 (in Chinese)
9. Guan X, Wang X, Zhu Z, Zhang L, Fu H. Ground vibration test and dynamic response of horseshoe-shaped pipeline during tunnel blasting excavation in pebbly sandy soil. Geotechnical and Geological Engineering, 2020, 38(4): 3725−3736
10. Yang G, Wang G, Lu W, Zhao X, Yan P, Chen M. Numerical modeling of surface explosion effects on shallow-buried box culvert behavior during the water diversion. Thin-walled Structures, 2018, 133(9): 153−168
11. Jiang F, Dong S, Zhao Y, Xie Z, Guedes Soares C. Investigation on the deformation response of submarine pipelines subjected to impact loads by dropped objects. Ocean Engineering, 2019, 194: 106638
12. He S W, Qu Z, Ye L H. Experimental study on seismic vulnerability of common water supply pipelines in buildings. China Civil Engineering Journal, 2018, 51(10): 11−19 (in Chinese)
13. Cui W, Song H F, Zhang S R. Numerical analysis of water conveyance safety of large box culvert under impact load. Journal of Vibration and Shock, 2012, 31(22): 188−192 (in Chinese)
14. Shahrin M I, Abdullah R A, Jeon S, Jeon B, Sa'ari R. Numerical simulation of rock fragmentation by blasting using Discrete Element Method and Particle Blast Method. IOP Conference Series. Materials Science and Engineering, 2019, 527(1): 012032
15. Xia Y, Jiang N, Zhou C, Luo X. Safety assessment of upper water pipeline under the blasting vibration induced by Subway tunnel excavation. Engineering Failure Analysis, 2019, 104: 626−642
16. Jiang N, Zhu B, He X, Zhou C, Luo X, Wu T. Safety assessment of buried pressurized gas pipelines subject to blasting vibrations induced by metro foundation pit excavation. Tunnelling and Underground Space Technology, 2020, 102: 103448
17. Zhang Z, Zhou C B, Lu S, Jiang N, Wu C. Dynamic response characteristics of adjacent buried concrete pipelines under blasting vibration. Journal of Harbin Institute of Technology, 2017, 46(9): 79−84
18. Zhu B, Jiang N, Zhou C, Luo X, Li H, Chang X, Xia Y. Dynamic interaction of the pipe-soil subject to underground blasting excavation vibration in an urban soil-rock stratum. Tunnelling and Underground Space Technology, 2022, 129: 104700
19. Zhu B, Jiang N, Zhou C, Luo X, Yao Y, Wu T. Dynamic failure behavior of buried cast iron gas pipeline with local external corrosion subjected to blasting vibration. Journal of Natural Gas Science and Engineering, 2021, 88: 103803
20. Zhang Y Q, Jiang N, Jia Y S, Zhou C B, Luo X D, Wu T Y. Blasting vibration response characteristics of high density polyethylene pipe in water filled state. Journal of Zhejiang University (Engineering Science), 2020, 54(11): 2120−2127 + 2137 (in Chinese)
21. Zhu B, Jiang N, Jia Y S, Zhou C B. Field experimental study on blasting vibration effect of Underpass gas pipeline. Journal of rock mechanics and engineering, 2019, 38(12): 2582−2592
22. Guan X M, Zhang L, Wang L M, Fu H X, Yu D M. Blasting vibration characteristics and safety standard of tunnel short distance underpass pipeline. Journal of Central South University, 2019, 50(11): 2870−2885 (in Chinese)
23. Xia Y Q, Jiang N, Zhou C B, Sun J S. Study on dynamic response characteristics of water supply pipeline under blasting vibration of Underpass subway tunnel. Blasting, 2019, 36(1): 6−13+37 (in Chinese)

24. Zhu B, Jiang N, Zhou C B, Wu T Y. Study on dynamic response characteristics of adjacent pressure gas pipeline under blasting action of excavation of foundation pit. Journal of Vibration and Shock, 2020, 39(11): 201−208 (in Chinese)
25. Jiang N, Zhu B, Zhou C, Luo X, Li H, Wu T, Lyu G. Safety criterion of gas pipeline buried in corrosive saturated soft soil subjected to blasting vibration in a coastal metro line. Thin-walled Structures, 2022, 180: 109860
26. Yin T, Zhou C B, Zheng C Q, Jiang N, Chen Z G. Dynamic response characteristics of blasting strata in silt-rock stratum under different working conditions. Journal of Vibration and Shock, 2021, 40(11): 269−276 (in Chinese)
27. Lyu G, Zhou C, Jiang N. Experimental and numerical study on tunnel blasting induced damage characteristics of grouted surrounding rock in fault zones. Rock Mechanics and Rock Engineering, 2022, 1(15): 03055
28. Zhao K, Jiang N, Zhou C, Li H, Cai Z, Zhu B. Dynamic behavior and failure of buried gas pipeline considering the pipe connection form subjected to blasting seismic waves. Thin-walled Structures, 2022, 170: 108495
29. Peng M, Shi C, Chen J. Safety of buried pipeline under coupling effect of tunnel excavation and blasting disturbance. Journal of Vibration and Shock, 2021, 40(19): 193−199 (in Chinese)
30. Wu T, Jiang N, Zhou C, Luo X, Li H, Zhang Y. Experimental and numerical investigations on damage assessment of high-density polyethylene pipe subjected to blast loads. Engineering Failure Analysis, 2022, 131: 105856
31. Abuhajar O, El Naggar H, Newson T. Experimental and numerical investigations of the effect of buried box culverts on earthquake excitation. Soil Dynamics and Earthquake Engineering, 2015, 79: 130−148
32. Cui Z, Lu S S, Song H F, Zhang D Y. Sph-fem coupling analysis of safety of large box culvert under blast load. Journal of Tianjin University Science and Technology, 2012, 45(9): 838−844 (in Chinese)
33. GB 50010-2010. Code for Design of Concrete. Beijing: General Administration of Quality Supervision, Inspection and Quarantine of the People's Republic of China, 2010 (in Chinese)